RESEARCH ARTICLE NEURODEGENERATION

ApoE isoform– and microbiota-dependent progress generation in a mouse model of tauopathy

DONG-OH SEO, DAVID O'DONNELL, [...], AND DAVID M. HOLTZMAN +20 authors Authors Info & Affiliations

SCIENCE 13 Jan 2023 Vol 379, Issue 6628 DOI: 10.1126/science.add1236

Microbiota and tau-mediated disease

The accumulation of certain forms of the tau protein in the brain is linked to loss of n
and cognitive decline in Alzheimer's disease and several other neurodegenerative dis
(APOE), the strongest genetic risk factor for Alzheimer's disease, regulates brain infla
mediated brain damage; however, the gut microbiota also regulates brain inflammati
tau-mediated brain injury, Seo *et al*. found that manipulation of the gut microbiota re
tion of inflammation, tau pathology, and brain damage in a sex- and APOE-dependen
Perspective by Jain and Li). —SMH

Structured Abstract

INTRODUCTION

Alzheimer's disease (AD) is characterized by early deposition of amyloid-β (Aβ) plaqu
cal tau accumulation. Although Aβ is a necessary factor in AD pathogenesis, its accu
insufficient for neurodegeneration and cognitive decline. By contrast, pathological ta
linked with neurodegeneration and cognitive decline in AD and primary tauopathies.
crobiota have been reported in AD, which suggests that the microbiota may contribut
Animal studies to date have focused mainly on how gut microbiota alterations affect
tauopathy and neurodegeneration. Additionally, recent studies have suggested that a
isoforms, which strongly influence AD risk and regulate tau-mediated neurodegenera
the gut microbiota. Therefore, further investigations to characterize the contribution
tauopathy and neurodegeneration are important.

RATIONALE

We assess the hypothesis that the gut microbiota regulates tau pathology and tau-me
tion in an ApoE isoform–dependent manner. A mouse model of tauopathy (*P301S* tau
pressing human ApoE isoforms (ApoE3 and ApoE4), referred to as TE3 and TE4, was s
lation of the gut microbiota using two approaches: (i) being raised in germ-free (GF)
term antibiotic (ABX) treatment early in life. Animals were fed a standard mouse cho
thanasia at 40 weeks of age, when this mouse model typically has severe brain atroph

RESULTS

The gut microbiota manipulations resulted in a notable reduction of tau pathology an
an ApoE isoform–dependent manner. Both male and female GF TE4 mice showed a m
atrophy compared with conventionally raised (Conv-R) mice. Conv-R ABX-treated TE

vide an avenue to further explore the prevention or treatment of AD and primary tau

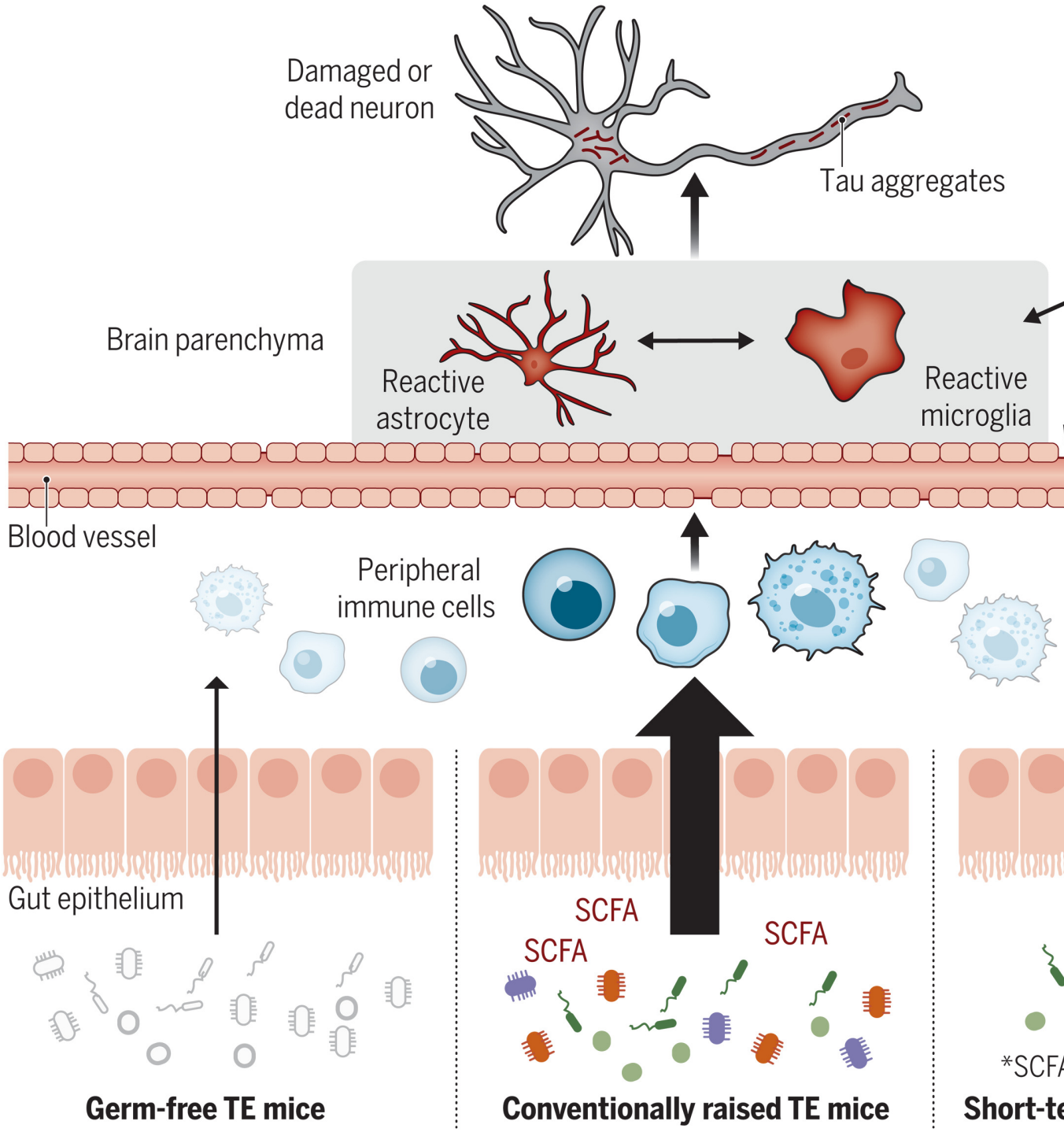

P301S tau transgenic mice expressing human APOE (TE mice).
The dysregulated gut-brain axis and its effect on tauopathy and tau-mediated neurodegeneration. Dysbios
composition (bottom center), contributes to tau-mediated neurodegeneration by generating bacterial met
ence peripheral immune cells. These cells promote central nervous system (CNS) inflammation and contr
neurodegeneration. Short-term antibiotics (bottom right) or germ-free conditions (bottom left) reshape or
reduce their metabolites. These microbiota manipulations influence effects of peripheral immune cells on
mediated neurodegeneration. ApoE4 in the CNS exacerbates local toxicity and blood-brain barrier dysfunc

Abstract

Tau-mediated neurodegeneration is a hallmark of Alzheimer's disease. Primary tauop

RELATED PERSPECTIVE

Gut microbes modulate neurodegeneration

Alzheimer's disease (AD) is a fatal, progressive neurodegenerative disease, characterize amyloid-β (Aβ) plaques followed by pathological tau accumulation in the limbic system which is strongly linked to neuronal loss and brain atrophy (1). Evidence is mounting th gut microbiota perturbations and Aβ deposition, potentially through effects on neuroin homeostasis (2–4). However, the contribution of the gut microbiota to tau-mediated ne strongly correlated with cognitive decline in AD and other tauopathies, has not been ch recent studies have reported that the configuration of the gut microbiota is differential tein E (APOE), the strongest genetic risk factor for AD and a known regulator of tau-me (5, 6). We used a mouse model of tauopathy with animals expressing different human A hypothesis that the gut microbiota regulates tau-mediated neurodegeneration in an Ap manner.

TE4 germ-free mice are protected against tau-mediated neuro

We began by rearing genetically engineered C57BL6J mice containing a *P301S* human ta and a knocked-in human *APOE4* gene (*Tau/APOE4*, abbreviated TE4) (7) under germ-fre group of TE4 mice was exposed to microbes originating from their TE4 dams beginning ally raised (Conv-R) mice were subsequently maintained under specified pathogen-free rier facility. A third group of mice was reared under GF conditions until 12 weeks of age gavage of fecal microbiota sampled from 40-week-old Conv-R TE4 (Ex-GF) mice (Fig. 1A standard rodent chow rich in plant polysaccharides. We euthanized animals from all gro time point when Conv-R TE4 mice display substantially greater tau-mediated neurodeg (i) Conv-R P301S mice harboring other human APOE isoforms in their genomes or (ii) C mouse and human APOE (7, 8). Unless otherwise indicated, all analyses were performed tained from 40-week-old mice.

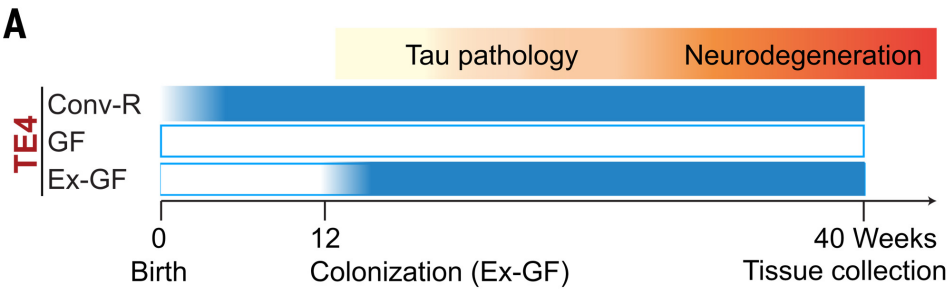

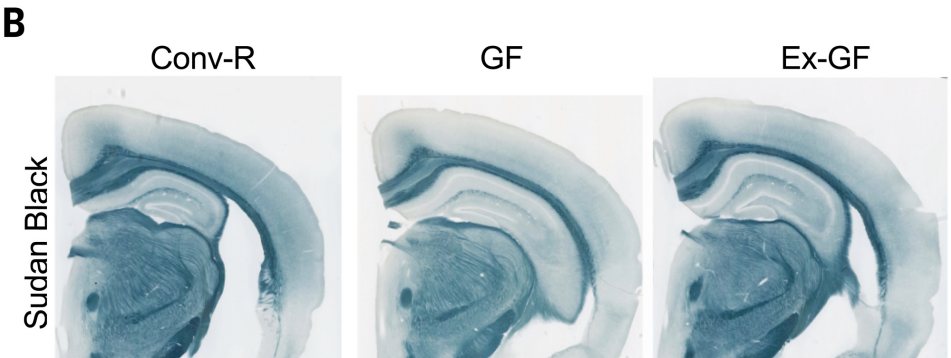

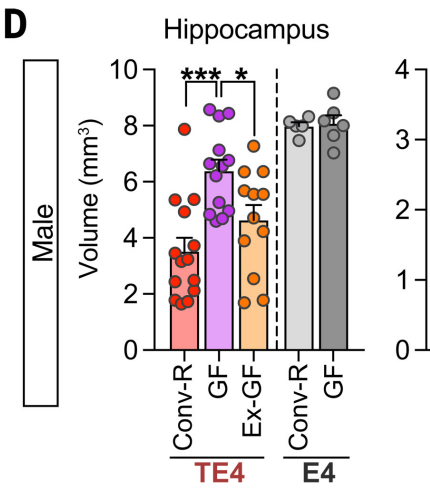

Conv-R male and female TE4 mice displayed severe regional brain atrophy, manifested
and lateral ventricle (LV) enlargement relative to E4 mice lacking the tau transgene (Fig
male and female TE4 mice had significant preservation of brain tissue compared with t
parts, as judged by hippocampal and LV sizes as well as by measurements of hippocamp
ness—a direct estimate of neuronal loss (fig. S1, C and D). Comparison of these areas of
week-old TE4 mice provided evidence that the protective effect produced by the GF stat
progression of neurodegeneration (fig. S1, E and F). We did not detect rescue from neur
entorhinal-piriform cortex of GF TE4 animals (fig. S1G).

The GF rescue from neurodegeneration was reversed when animals were colonized with
ties harvested from sex-matched Conv-R TE4 animals (fig. S1, H to J); 28 weeks after co
GF mice exhibited hippocampal and LV volumes and hippocampal neuronal layer thickn
documented in Conv-R mice (Fig. 1, B and D, and fig. S1D). Staining brain sections with
(AT8) revealed a marked decrease in tau phosphorylation in 40-week-old GF compared
mice (Fig. 1, C and E). By contrast, we did not observe any differences in hippocampal A
week-old GF and 12-week-old Conv-R mice (fig. S1, K and L). Thus, the microbiota grea
ance of tau-mediated neurodegeneration.

TE4 GF mice exhibit reduced reactive gliosis

Although elevated levels of pathological phosphorylated tau (p-tau) may directly contri
tion and death, there is strong evidence that reactive microglia and astrocytes are requi
rodegeneration (*7*, *9*–*11*). Recent studies have indicated that the gut microbiota contrib
(*12*–*14*), leading us to hypothesize that the microbiota may modulate tau-mediated neu
model by altering glial reactivity. Therefore, we first stained brain sections with marker
croglia [glial fibrillary acidic protein (GFAP), Iba1, and CD68]. Consistent with the amou
sion of all these glial markers in the hippocampus was strongly reduced in GF compared
(Fig. 2, A and B). Furthermore, analysis of glial morphology in the hippocampus (fig. S2
trocytes in GF mice were larger with more branched processes compared with those in C
phological alterations of glial cells in GF mice were also observed at 12 weeks of age, wh
pathology but no evidence for neurodegeneration (fig. S3).

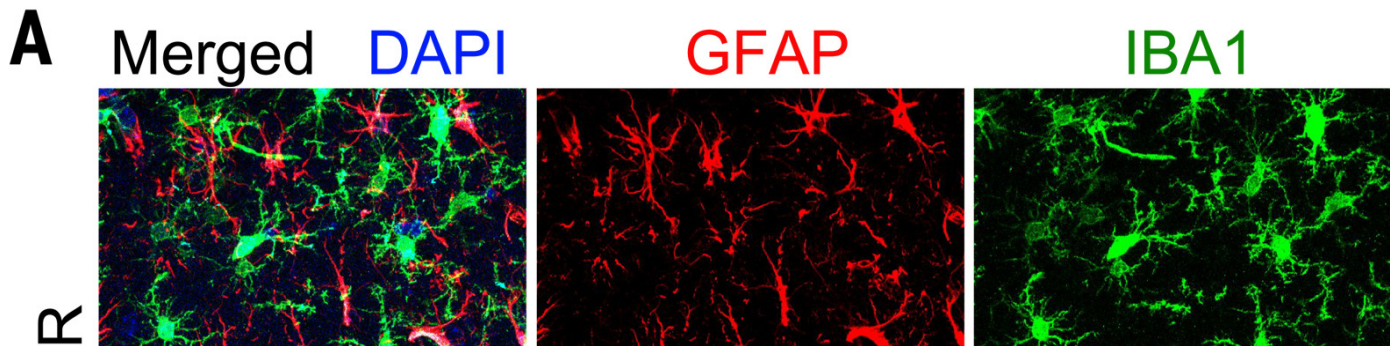

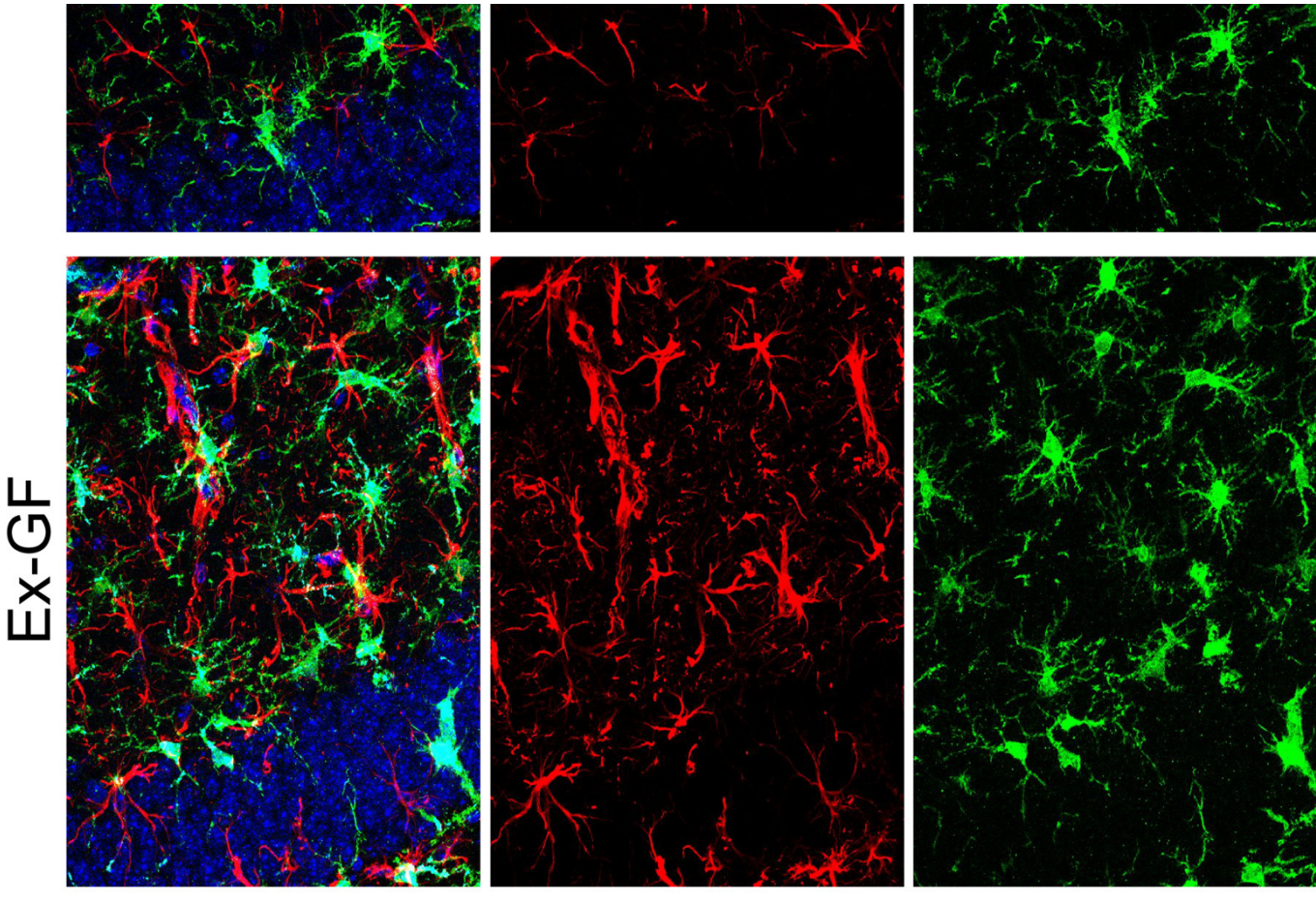

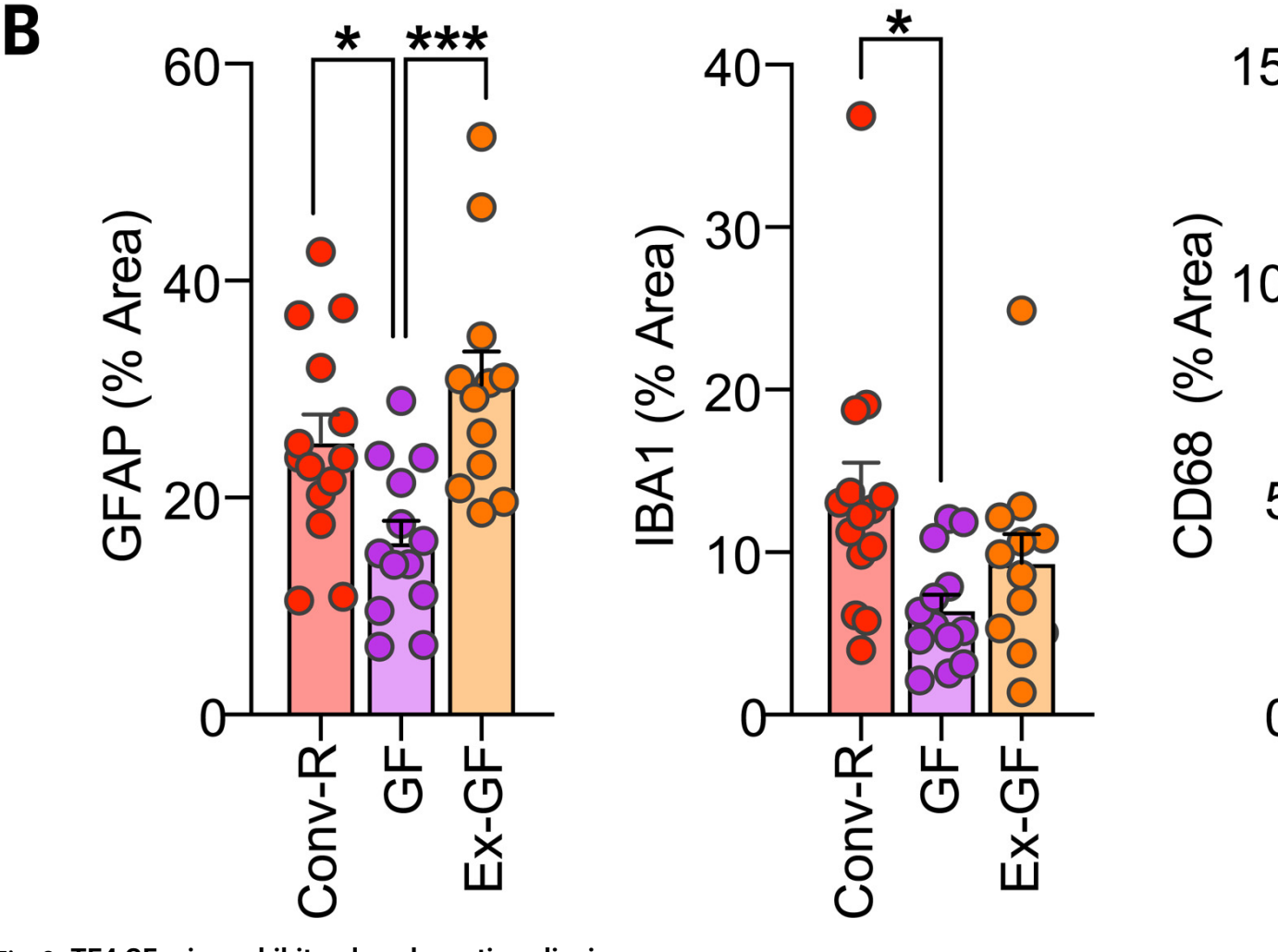

Fig. 2. TE4 GF mice exhibit reduced reactive gliosis.

(**A**) Representative immunofluorescence images of hippocampal sections from 40-week-old male Conv-R, G
tibodies to GFAP (red), Iba-1 (green), and CD68 (cyan) as well as DAPI (blue). Scale bar, 25 µm. GCL, granule
of sections taken from the hippocampus covered by GFAP (left), Iba-1 (middle), and CD68 (right) staining. M

decreased expression, respectively, in these modules were tightly linked to the protecti
(fig. S4, G to J). Thus, GF conditions affect microglia and astrocyte reactivity or activati
mediated neurodegeneration.

Antibiotic-induced gut microbiota perturbation protects agains
neurodegeneration

To test whether the gut microbiota regulates tau-mediated neurodegeneration in an Ap
manner, we treated groups of Conv-R TE4 mice, *P301S* tau transgenic mice expressing h
P301S tau animals without APOE (TEKO) with an antibiotic cocktail (ABX) composed o
colistin, metronidazole, and vancomycin (*4*). Gavage with the antibiotic cocktail (or wat
occurred daily from postnatal days 16 to 22. The fecal microbiota was serially sampled,
nized at 40 weeks of age (Fig. 3A). The short-term ABX treatment produced a marked, i
total number of viable bacteria; although this decrease in viability was transient, cultur
disclosed that the proportional representation of various bacterial taxa in the microbio
remained different from controls throughout life (see fig. S5, A to E, and below).

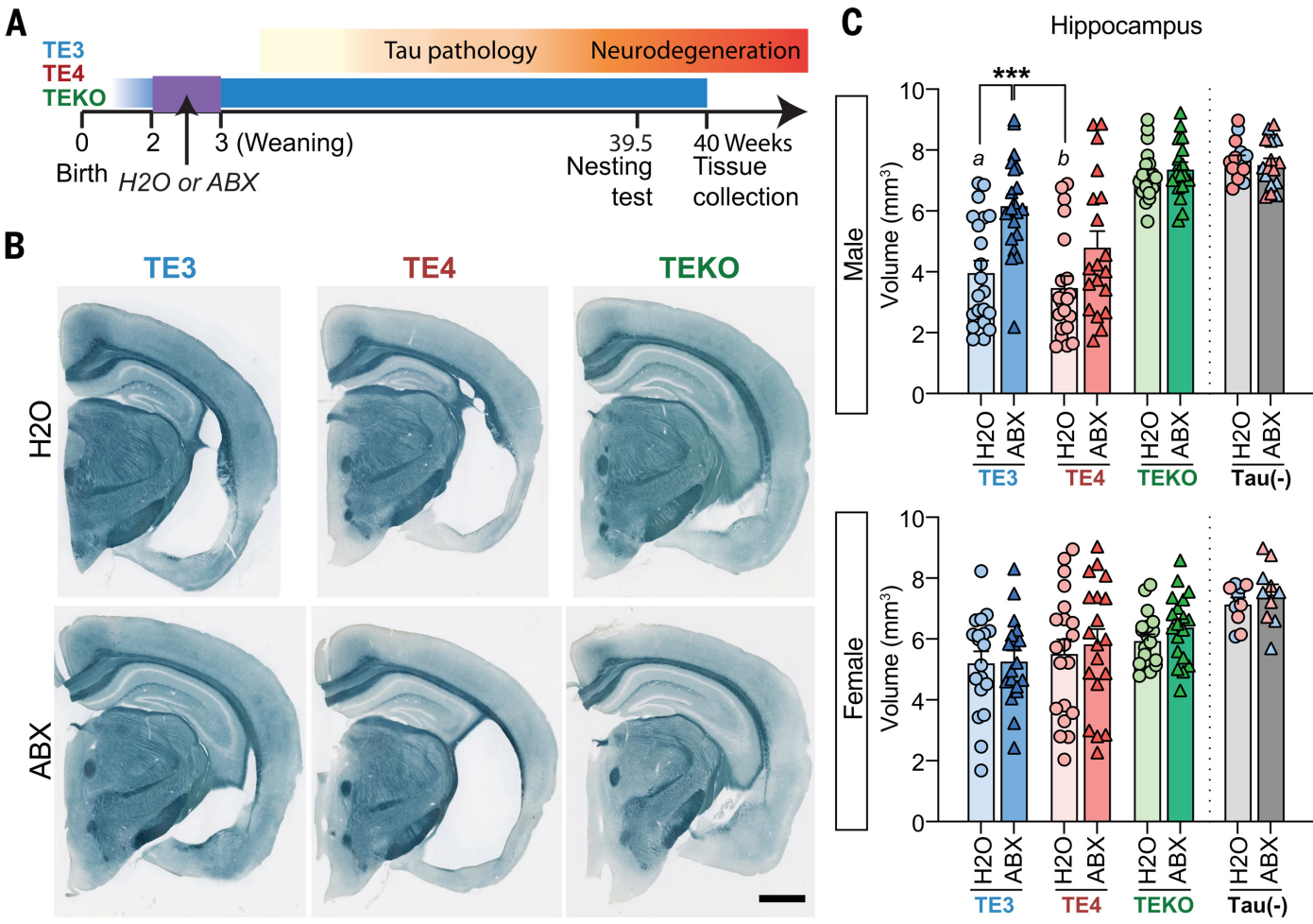

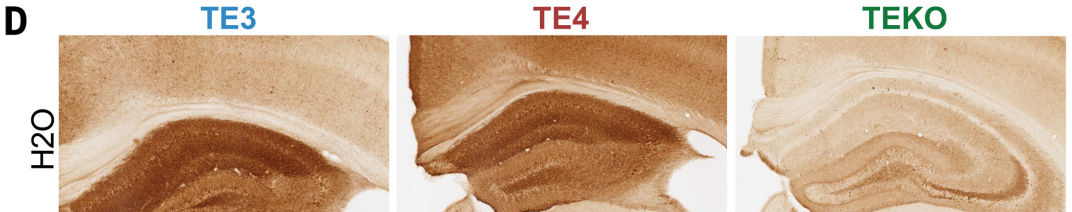

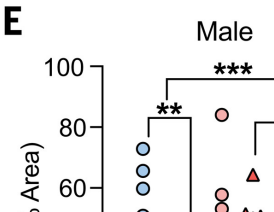

Volumetric analysis revealed that 40-week-old male mice in the H_2O-treated control gr
H_2O animals) had statistically significant hippocampal atrophy compared with mice lac
(Fig. 3, B and C) (*8*). However, TE3-ABX but not TE4-ABX mice showed significant hippo
tive to controls. Enlargement of the LV and entorhinal-piriform cortical atrophy were a
by ABX treatment independent of APOE genotype, but the degree of ABX effect was hig
TE4 mice in general (i.e., the $\log_2$ fold changes by ABX in the LV size were −0.86 in TE3
$\log_2$ fold changes by ABX in the entorhinal-piriform cortex size were 0.57 in TE3 and 0.
fig. S5F). ABX treatment also prevented thinning of hippocampal neuronal cell layers in
type (fig. S5G). These phenotypic effects of ABX treatment were seen in TE3 and TE4 m
cept in the case of the CA1 pyramidal layer, which was slightly, albeit significantly, thic
and females (fig. S5G). In concert with hippocampal brain atrophy, male TE3-ABX mice
AT8 staining relative to male TE3-H_2O mice (Fig. 3, D and E).

ABX treatment did not influence brain volume or early tau pathology in 12-week-old m
K). At 40 weeks of age, analysis of male cortical tissue also revealed that ABX treatment
detergent-soluble fraction (RIPA) and both p-tau and human tau levels in the insoluble
three APOE genotype groups (fig. S6). Furthermore, nest-building behaviors, known to
pus damage and neurodegenerative disease (*15*), showed significant improvement in ma
treated with ABX, which correlated with hippocampal volumes (fig. S7).

Antibiotic treatment alters astrocyte and microglial gene expr
logical responses

Single-nucleus RNA sequencing (snRNA-seq) of hippocampal tissue collected from Con
belonged to all three APOE genotype groups and were not exposed to antibiotics identi
which were categorized into excitatory and inhibitory neurons, astrocytes, microglia, o
dendrocyte progenitor cells (fig. S8, A and B). Cell proportion analysis showed that cert
(e.g., exc1, exc2, and exc5) were reduced in the presence of tau pathology and expanded
in agreement with the hippocampal volumetric data. The astrocyte population was redu
the presence of tau pathology. The microglial population, which expanded approximate
tion) with tau pathology, was reduced two- to threefold with ABX treatment.

The astrocyte cluster was rescaled and reclustered, revealing four subclusters (astro0 to
S8C). Reclustering of the microglia cluster identified three subclusters (micro0 to micro
pathology resulted in a strong shift from astro0 to astro1 and micro0 to micro1. ABX tre
shifts in TE3 but not TE4 male mice, consistent with a stronger protective effect with A
pared with TE4 male mice. Further differentially expressed gene (DEG) analysis betwee
with pathological shifts revealed that the top up-regulated pathways in astrocyte subcl
tro0; data S5) were associated with GO terms related to gliogenesis and cellular chemic

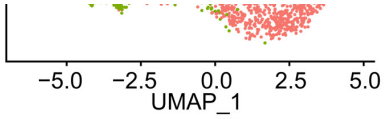
−5.0
−2.5
0.0
2.5
5.0
UMAP_1

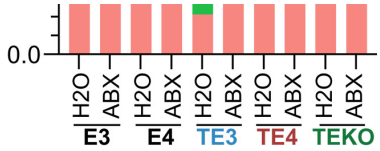
0.0
H2O
ABX
E3
E4
TE3
TE4
TEKO

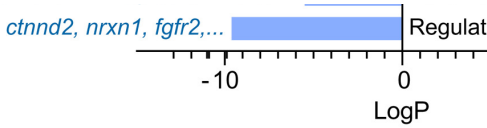
ctnnd2, nrxn1, fgfr2,...
Regulat
-10
0
LogP

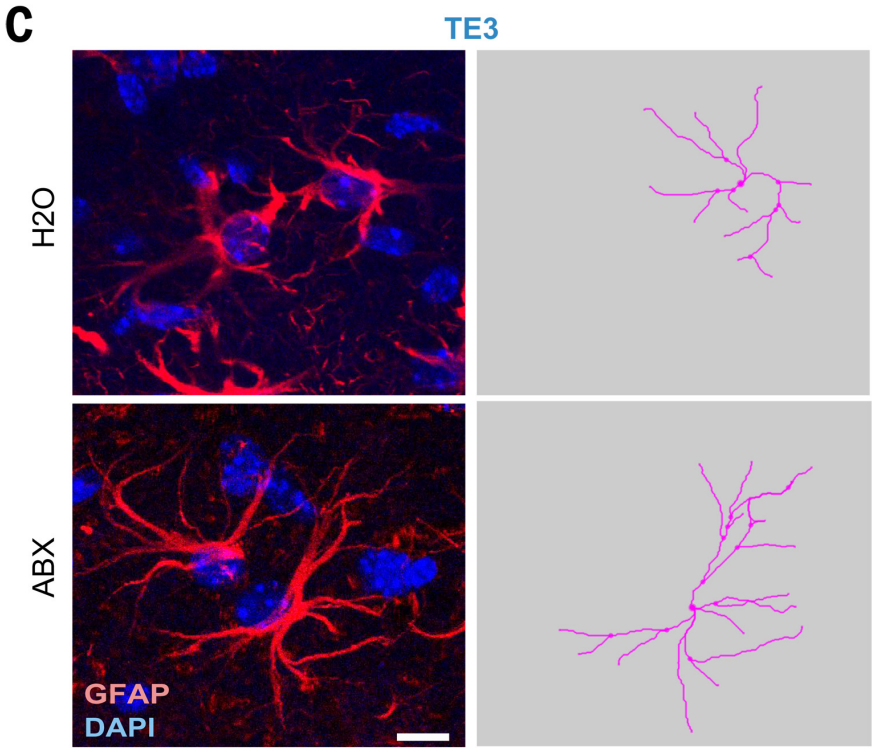
C
TE3
H2O
ABX
GFAP
DAPI

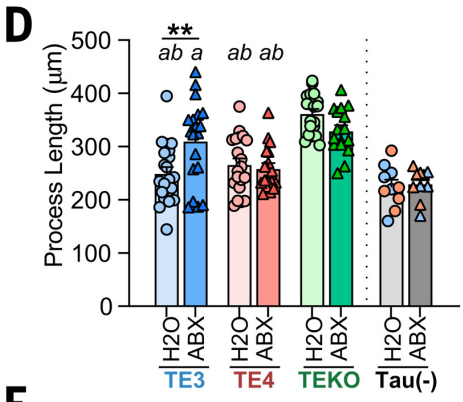
D
Process Length (μm)
500
400
300
200
100
0
**
ab a
ab ab
H2O
ABX
TE3
TE4
TEKO
Tau(-)

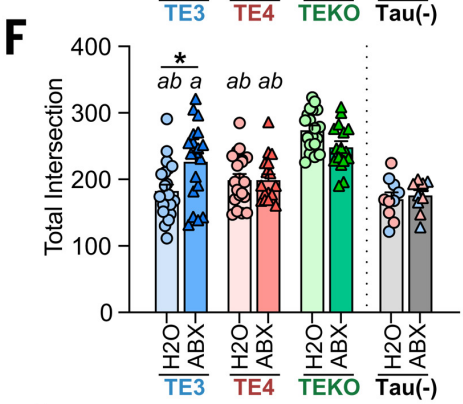
F
Total Intersection
400
300
200
100
0
*
ab a
ab ab
H2O
ABX
TE3
TE4
TEKO
Tau(-)

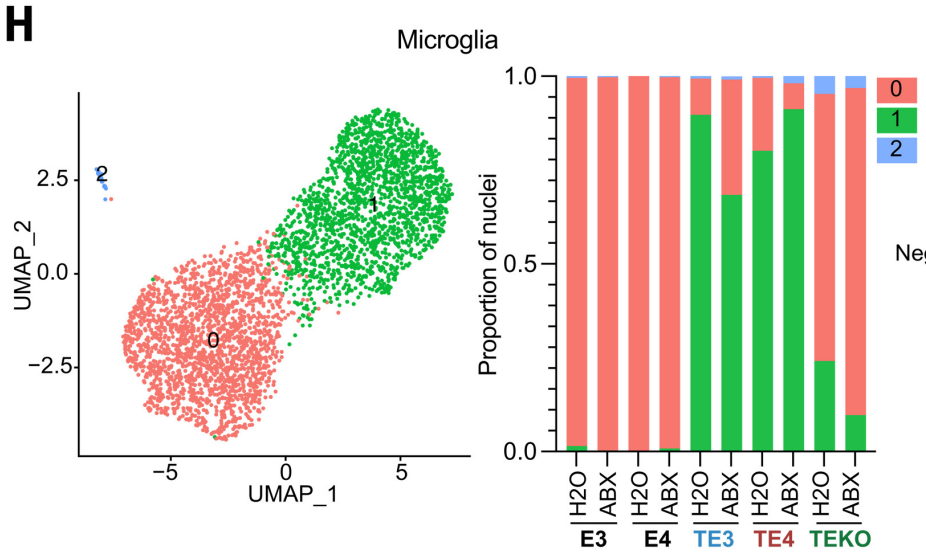
H
Microglia
UMAP_2
2.5
0.0
−2.5
−5
0
5
UMAP_1
Proportion of nuclei
1.0
0.5
0.0
0
1
2
H2O
ABX
E3
E4
TE3
TE4
TEKO

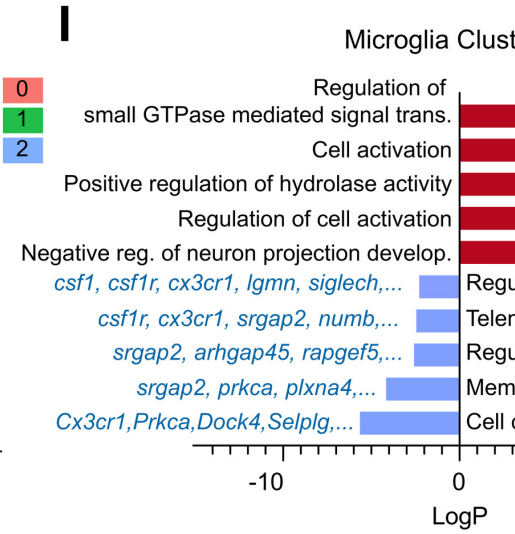
I
Microglia Clust
Regulation of
small GTPase mediated signal trans.
Cell activation
Positive regulation of hydrolase activity
Regulation of cell activation
Negative reg. of neuron projection develop.
csf1, csf1r, cx3cr1, lgmn, siglech,...
csf1r, cx3cr1, srgap2, numb,...
srgap2, arhgap45, rapgef5,...
srgap2, prkca, plxna4,...
Cx3cr1,Prkca,Dock4,Selplg,...
-10
0
LogP

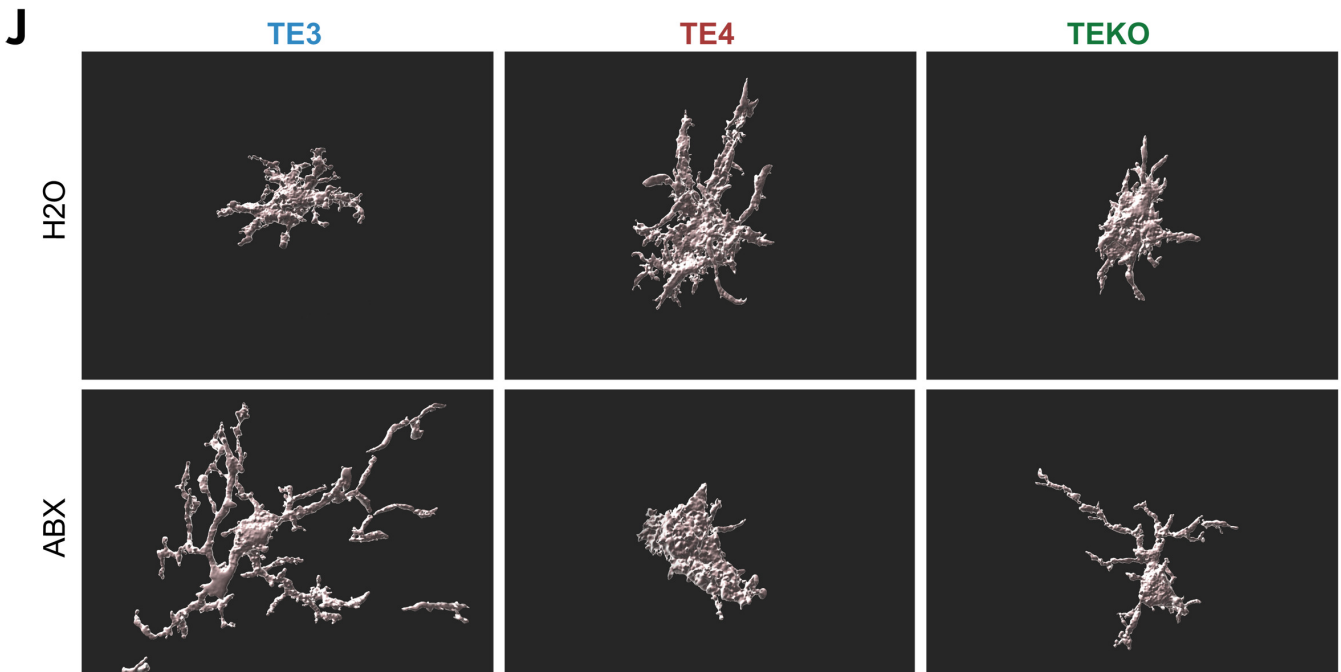
J
TE3
TE4
TEKO
H2O
ABX

performed GFAP, Iba1, and CD68 immunostaining. Although the coverage area of the i
veal significant ABX effects (fig. S10A), morphometric analysis revealed that ABX drove
a more homeostatic-like morphological state (e.g., increased length of processes and si
but not in male TE4 and TEKO, female TE3, or male 12-week-old TE3 mice (Fig. 4, C to
to K). Thus, ABX-induced perturbation of the microbiota protects against tau-mediated
strongly in male TE3 mice, and this effect is manifested by changes in multiple cell type
microglia.

Antibiotic treatment reshapes the bacterial communities and r
fatty acids

The microbiota perturbation induced by ABX was evidenced by (i) measurements of cec
body weight (known to be markedly increased in GF compared with Conv-R animals and
mice; fig. S1, A and B, and fig. S5, D and E) and (ii) culture-independent analysis of the
terial taxa in feces. The latter approach was based on sequencing PCR amplicons genera
of bacterial 16*S* ribosomal RNA (rRNA) genes [amplicon sequence variants (ASVs)] and
taxonomic bins. Alterations in alpha and beta diversity as well as the representation of
groups are summarized in figs. S11 to S13. Phylum- and genus-level changes in ABX-tre
ferent from H_2O-treated controls up to the time of euthanasia (fig. S11, D and E).

Linear discriminant analysis revealed that the members of the genera *Helicobacter*, *Rum*
Butyricicoccus had lower relative abundance in the fecal microbiota of ABX-treated grou
form groups (Fig. 5A and fig. S12, A to C) but not in female TE3 mice (Fig. 5B and fig. S1
suggested that the microbiota modulates glial activation through the production of mic
short-chain fatty acids (SCFAs) (*12*, *13*). *Ruminococcus* and *Butyricicoccus* are associated
Also, the relative abundance of several bacterial family-level taxa known to produce SC
Ruminococcaceae and *Lachnospiraceae*, were reduced with ABX across APOE genotypes
tion of these taxa was greater in male compared with female members of the TE3-H_2O t
and lower in TE3 compared with TE4 mice (fig. S13, B and C). Gas chromatography–mas
cecal samples disclosed that, consistent with our observation that SCFA-producing bact
treatment in males, acetate, propionate, and butyrate were significantly reduced across
correlating with biomarkers of tau pathology (Fig. 5, D and E, and fig. S13A), but not in

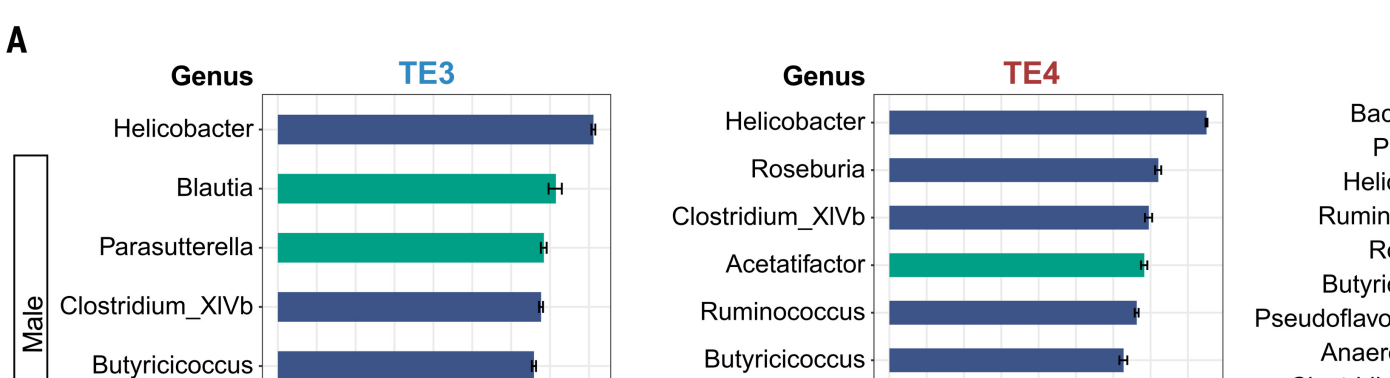

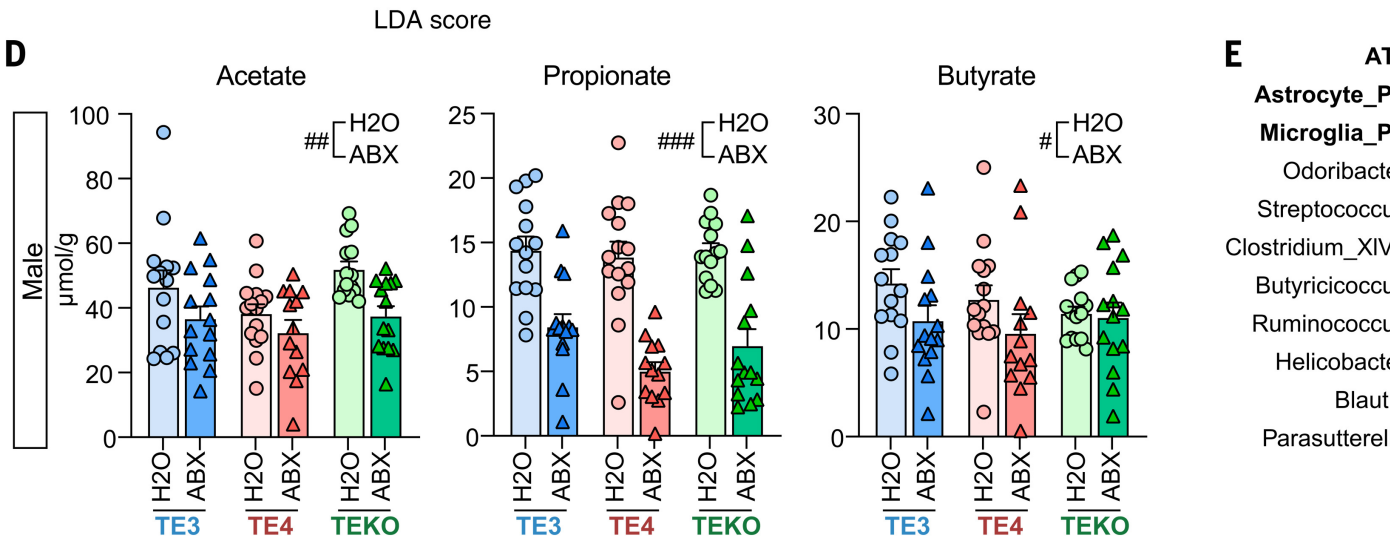

Fig. 5. Effects of ABX treatment on fecal microbiota composition and cecal levels of SCFAs.
(**A** and **B**) Linear discriminant analysis (LDA) scores. Horizontal bars represent the LDA scores for each genu and TEKO mice (A) and in female TE3 mice (B). Indigo and green bars represent taxon features with signific belonging to the control H_2O and versus ABX treatment groups, respectively (LDA scores > 2). (**C**) Comparis between 40-week-old male and female TE3-H_2O mice. Family and genus assignments are shown. (**D**) Target

ABX-induced gut microbiota perturbation alters the peripheral and the effects of SCFA on TE4 GF mice

It is unclear whether SCFAs act directly on glial cells because SCFA receptor–encoding g expressed in glial cells (12). However, we postulated that SCFAs could affect other inflar mune cells that directly access the brain or the immune milieu around the brain (i.e., th ductions in meningeal natural killer (NK) and plasmacytoid dendritic cells (pDC) cells i Furthermore, γδ T and pDC cells were reduced in GF mice (fig. S14, A to C). These latte cytokines, such as interleukin-17 (IL-17), interferon (IFN) type-I, and others, which ma in the brain (17–19).

Multiplex cytokine profiling revealed that plasma levels of MCP-3, IL-2R, BAFF, and Eo duced by ABX in mice (fig. S15). The degree of reduction of Eotaxin, which can cross the activate glial cells, was greater in TE3 mice compared with those belonging to the other crobiota can modulate systemic immunity, including peripheral macrophages (20). ABX mice significantly altered lung alveolar macrophage gene expression (fig. S16). In turn, teraction with adaptive immune cells could potentially affect brain pathology. The cyto that some cytokines released by macrophages, such as IP-10 and BAFF, or those that ca such as MIP-1a, were affected by ABX treatment. Brain border innate and infiltration o

eration in male and female TE4 mice. ABX treatment is also neuroprotective, but its eff
and was greater in the presence of APOE3 compared with APOE4. Our results also sugg
sex differentially modulate the microbial response to ABX, resulting in significantly lov
microbiota-associated metabolic changes are associated with altered peripheral cytokir
changes in the innate immune response in the brain.

We hypothesize that the gut microbiota regulates the brain's innate immune response t
neurodegeneration in the brain. We speculate that in TE3 mice, the ABX-induced micro
duces peripheral immune activation may moderate the brain's innate immune response
tau-mediated neurodegeneration. By contrast, in TE4 mice, the microbiota-associated
were not altered as much by ABX treatment. It is possible that the gain of function of A
fects on the local innate immune response in the brain were stronger than that of APOI
mately failed to protect against tau-mediated neurodegeneration to the same degree. C
complete absence of the microbiota, even in TE4 mice, the depletion of microbially pro
mune signals results in a strong reduction of the disease-associated astrocyte and micr
to a decrease in tau-mediated neurodegeneration (consistently, SCFA supplementation
and tau pathology in TE4 GF mice).

Further studies are needed to test these hypotheses and to gain greater understanding
nipulation, microbiota-linked metabolites, central or peripheral immune response, and
rodegeneration are related. A starting point for these follow-up analyses could involve
with gut microbiota harvested from Conv-R mice with different sex, age, and ApoE isof
donors (with or without tau-mediated neurodegeneration). It is possible that the TE4 G
ferent types of microbiota (e.g., harvested from wild-type mice, not necessarily from TE
verse the GF rescue from neurodegeneration. It may be that the host genetic makeup in
the effects of the transferred microbiota composition derived from a more general bacte
ficient to activate the metabolic-neuroinflammation axis. Alternatively, the sex, age, Ap
state of neurodegeneration may be critical in regard to the source from which the trans
rived. Future studies are needed to sort out these possibilities. Nonetheless, these resul
gut microbiota targeting may provide ways to prevent or treat progression of AD and pr

Materials and methods

Animals

All animal experiments were performed using protocols approved by the Institutional A
Committee (IACUC) at Washington University School of Medicine. All phenotyping and
formed by researchers who were completely blind to the experimental hypothesis and t

P301S tau transgenic mice (PS19tg; Stock No. 008169, Jackson Laboratories) contain a t

cut ind and a polycarbonate inner top containing a filter insert.

Conv-R TE4 mice were rederived as GF by embryo transfer. Embryos were harvested 1 d
ferred under sterile conditions to a pseudopregnant GF mother generated by mating to
The transgenic GF descendants were intercrossed to produce TE4 GF mice. GF animals
ble film gnotobiotic isolators (Class Biologically Clean Ltd., Madison, WI). GF status wa
using universal bacterial 16*S* rRNA gene primers and by culturing fecal and skin swabs.
of Conv-R mice were used as controls.

GF mice were colonized with fecal microbiota samples collected from 40-week-old Conv
GF animals. To do so, fecal samples from 4 to 5 mice per sex were pooled, homogenized
phosphate-buffered saline (PBS) containing 0.05% cysteine-HCL and 20% glycerol (5 pe
−80°C until the time of the fecal microbiota transplantation. A 200-μL aliquot of the res
thawed and administered to sex-matched 12-week-old GF mice by oral gavage on two o
4-day interval. The Ex-GF mice were maintained in plastic flexible film gnotobiotic isol
Clean Ltd., Madison, WI) (2 to 5 mice of the same sex per cage).

All Conv-R, GF, and Ex-GF mice (2 to 5 mice of the same sex per cage) were given the sa
(Teklab certified global 18% protein rodent diet; catalog no. T2018SC.15) ad libitum. Al
under a strict light cycle (lights on at 0600 hours and off at 1800 hours). Fresh fecal pell
collected directly in sterile 2-mL centrifuge tubes (Axygen; SCT-200-SS-R-S) and imme
the time of DNA extraction. All fecal pellet samples were collected at between 1500 hou
mize circadian rhythm effects.

Antibiotic treatment

Pups assigned to the ABX treatment group were gavaged with 100 μL of an antibiotic co
mg/mL kanamycin (Sigma-Aldrich K4000), 0.35 mg/mL gentamicin (Sigma-Aldrich G19
(Sigma-Aldrich C4461), 2.15 mg/mL metronidazole (Sigma-Aldrich M1547), and 0.45 m
Aldrich V2002) (prepared using autoclaved water). Gavage occurred daily from postnata
feeding needles (Cadence; catalog no. 7901). Control mice were gavaged with 100 μL of
gavage, mice were transferred to a new sterile cage to avoid contamination from accum
cages.

Nest-building behavior

A few days before euthanasia, group-housed mice were switched to individual housing
(2.5 g; no. NES7200, Ancare, Bellmore, NY) were introduced into each cage at ~1600 ho
1000 hours, the remaining nestlet was weighed. A 5-point scale was used to score the re
based on the percentage of nesting material remaining plus the shredding conditions: s
<25%; 2, nest shredding 25 to 50%; 3, nest shredding 50 to 90%; 4, nest shredding >90%
pacted yet; 5, complete nest built (fig. S7A).

NanoZoomer microscope (Hamamatsu); areas of interest were traced and measured in e
viewer (Hamamatsu). Volume was calculated by the sum of area × 0.3 mm (7, 8). All stai
obtained were performed by someone who was blind to the experimental hypothesis an
mals being assessed.

Neuronal layer thickness measurement

Left hemi-brain sections from each mouse, corresponding approximately to bregma coo
were mounted and stained in cresyl violet for 5 min at room temperature (7). Slices wer
in 50%, 70%, 95% (three times), and 100% ethanol (twice) (1 min per treatment) then cl
(twice), and cover-slipped in cytoseal60 (Thermo Fisher Scientific, catalog no. 8310-16)
Cytation 5 (Biotek) and analyzed with Gen5 Software (Biotek). Quantification of the thi
ular cell layer and the CA1 pyramidal layer were measured by drawing a scale line that c
areas each section and obtaining the average value. All staining and analysis of data ob
individuals blind to the experimental hypothesis and the treatments of the animals bei

Immunohistochemistry

Left hemi-brain sections, corresponding approximately to bregma coordinates −1.5 and
munohistochemistry. For AT8 staining, brain sections were washed in Tris-buffered sal
followed by incubation in 0.3% hydrogen peroxide in TBS for 10 min at room temperatu
TBS, sections were blocked with 3% milk in 0.25% TBS-X (Triton X-100) for 30 min follo
overnight with biotinylated AT8 antibody (Thermo Scientific, catalog no. 1020B, 1:500
ter washing three times with TBS, all sections were treated at room temperature for 60
in the VECTASTAIN Elite ABC-HRP Kit, followed by three washes in TBS. Finally, sectio
stained using ImmPACT DAB EqV Peroxidase Substrate. Slides were cover-slipped with
ing a Nanozoomer microscope at 20X magnification. Images were extracted by using th
with ImageJ software (National Institutes of Health, Bethesda, Maryland, USA, https://i

For immunofluorescence, sections were washed in TBS three times (5 min/cycle). After
blocked with a solution containing 3% BSA and 3% normal donkey serum in 0.25% TBS
perature, followed by an overnight incubation at 4°C with primary antibodies [mouse G
MAB3402, 1:1000), rabbit Iba1: Wako, (1:2000); rat CD68 (SeroTec, 1:500)]. The next da
TBS, slides were incubated with fluorescent-labeled secondary antibodies (Molecular Pr
room temperature. Sections were washed and incubated with 0.1% Sudan black solutio
washed once more, and mounted in ProLong Gold Antifade mounting medium (Molecu
were obtained by using a Leica Stellaris 5 confocal microscope and analyzed with Image

Brain tissue sample processing for enzyme-linked immunosorbent assay (ELISA)

Mouse posterior cortex was sequentially processed in (i) RAB buffer (100 mM MES, 1 ml
750 mM NaCl, 20 mM NaF, 1 mM Na_3VO_4, pH 7.0) supplemented with protease inhibitor
phosphatase inhibitors (PhosSTOP, Roche); (ii) RIPA buffer (150 mM NaCl, 50 mM Tris,

(mouse monoclonal, 150 ng/mL) for the human ApoE ELISA.

Astrocyte morphology analysis

Z-stacks (20 µm) of 4′,6-diamidino-2-phenylindole (DAPI)– and GFAP-labeled immuno acquired on a Leica Stellaris 5 confocal microscope with a 40X objective and 1024-pixel Simple Neurite Trace (SNT; ImageJ plug-in open-source tool) was used to reconstruct t GFAP-positive astrocytic main processes by semiautomatic tracing (26). For each mous domly selected in each section from two separate brain sections on the basis of GFAP-s a single DAPI-stained nucleus. The six astrocytes chosen from each mouse did not have edges of the field or were truncated. Fully traced astrocytes in SNT were used to obtain process length, end radius, the number of process branches, the total number of interac branches and radius from Sholl analysis (27), and the volume occupied by the astrocytic analysis (28).

Microglia morphology analysis

Z-stacks (20 µm) of Iba1-labeled immunofluorescence images were acquired on an LSM focal microscope (Zeiss) with a 60X objective, 1.8X zoom, and 1024-pixel by 1024-pixel a total of four z-stacks of the dentate gyrus region were taken from two separate brain s phology analysis was performed on three-dimensional (3D) images using Imaris 9.5 sof Morphology was analyzed using the Filament Tracer, with no loops allowed and spot de process start and end points per cell. Process reconstruction was made using the follow new starting points; largest diameter 9.00 µm, seed points 2.00 µm; remove seed points and diameter of sphere regions: 15 µm. All filament parameters were exported into sep analyzing the number of process branches, process length, and process volume per cell. construction, and data analysis were performed in a blinded manner with regards to the

Nanostring gene expression assay

RNA was isolated from mouse hippocampus using the RNeasy Mini Kit (QIAGEN, catalo trol checks were performed on all samples to determine RNA concentration and integri Nanostring gene expression assay, isolated RNA samples were processed by the Genom Washington University, using NanoString's nCounter Neuroinflammation panel (735 ge 770 targeted genes). Background noise in the data was corrected to a thresholding coun technical variation was corrected by using the geometric median value of the positive-c normalization was performed subsequently using the geNorm algorithm to select the o (*Mto1*, *Csnk2a2*, *Aars*, *Supt7l*, *Fam104a*, *Tbp*, *Ccdc127*, *Tada2b*, *Lars*, and *Cnot10*)

Differential gene expression was performed using nSolver 4.0 and the Advanced Analys Fold-change expression and *P* values were calculated by linear regression analysis using linear models. *P* values were corrected for multiple comparisons using the Benjamini-H Coexpression analysis was performed using the Weighted Gene Correlation Network An

cell debris removal step, centrifugation, and resuspension steps were repeated twice. O
and resuspension buffer was added in the last resuspension step. The resulting solution
Sucrose Cushion Buffer I [prepared by mixing 2.7 mL of Nuclei Pure 2M Sucrose Cushio
St. Louis) with 300 mL Nuclei Pure Sucrose Cushion Solution (MilliporeSigma, St. Louis
to the top of 500 µl Sucrose Cushion Buffer I in a 2-mL eppendorf tube]. After centrifug
min at 4°C, the nuclear pellet was resuspended in 500 µL nuclei wash and resuspension
of nuclei was determined using a Countess instrument (Invitrogen) and DAPI staining.
justed to 1200 nuclei/mL using nuclei wash and resuspension buffer before snRNA-seq.

Isolated nuclei were used for droplet-based snRNA-seq using the Chromium Single Cell
Genomics). Libraries were sequenced using a NovaSeq 6000 instrument (Illumina). Sam
processing, and single-nuclei 3′ counting was performed using the Cell Ranger Single-C
Genomics). Cell Ranger count was used to (i) align samples to a custom pre-mRNA refe
taining the human *APOE* gene, (ii) quantify reads, and (iii) filter those reads with a qual

The Seurat v3 and SoupX R packages were used for subsequent analysis of the datasets
cell-free RNA from each sample group was removed using SoupX. Nuclei with mitochon
gene counts <200 or >5000 were removed (Seurat). For each group, the percent of mitoc
as a nuisance variable, gene counts were normalized, and variable features identified us
tion in Seurat. The top 3000 variable genes were used to integrate experimental groups
PrepSCTIntegration, FindIntegrationAnchors, and IntegrateData commands in Seurat.
ysis (PCA) was performed on the integrated dataset and the first 30 principal componen
stream analysis using FindNeighbors. Clusters were identified using the FindClusters fu
ranging from 0.1 to 1.2. Final clustering was performed using a resolution of 0.3. The fi
were passed into UMAP using the RunUMAP command with default parameters. Differe
tween each cell cluster and all other clusters was performed on SCT data to identify ma
ual cell cluster. Clusters containing high mitochondrial genome content, or marker gen
cell type (i.e., microglia and excitatory neurons) were removed and data were reclustere
pal components and a resolution of 0.3. In total, 143,835 nuclei with a median UMI of 2
ber of 1664 across all 10 experimental groups were used in the final analysis.

Differential gene expression to identify marker genes was again performed using MAST
were identified on the basis of known cell type–specific markers. For subclustering anal
or microglia clusters were extracted from the dataset, RNA counts were renormalized, a
chondrial genes regressed out using the SCTransform command. PCA analysis was perf
reclustered. For astrocytes, in addition to regressing the percentage of mitochondrial g
(growth hormone) and Prl (Prolactin) transcripts were also regressed out due to detecti
ment group. The first 20 principal components were used, and clustering performed at
S5). For microglia, the first 10 PCs were used, and clustering performed at a resolution
genes for subclusters were identified using MAST (data S5 and S6). The SCTransform fu

(BioSpec Products) for 4 min with ~250 µl of 0.1 mm zirconia/silica beads and one 3.97-
trifugation at 3220 ×*g* for 4 min, 420 µL of the resulting aqueous phase was transferred
A 100 µL aliquot of the crude extract was mixed with 400 µL of a mixture of Qiagen buff
pH5.5 (675:45), and the mixture was passed through a Qiagen QiaQuick 96 plate by cen
min, washed twice with 900 µL of Buffer PE by centrifugation, and finally eluted with 1
DNA was quantified using Invitrogen Quant-iT dsDNA BR kit and normalized to 2 ng/µl
bacterial 16*S* rRNA gene was amplified by PCR using the following conditions: denatura
followed by 26 cycles of 94°C for 15 s, 50°C for 30 s, and 68°C for 30 s, followed by incub

Sample-associated 16*S* rDNA amplicons were quantified, pooled, and subjected to sequ
strument, paired-end 250 nt reads). Reads were demultiplexed, trimmed to 200 nucleot
by removal of chimeric sequences (DADA2 v. 1.13.0). ASVs were generated from demult
with DADA2 and taxonomy was assigned on the basis of the DADA2-formatted training
control and the resolution of ASVs were performed with the dada2 R package (*37*, *38*). A
to the kingdom Bacteria were filtered out. The remaining reads were assigned taxonom
Database Project (RDP trainset 16/release 11.5) 16*S* rRNA gene sequence database (*38*).

Analyses of alpha-diversity (richness, Faith's phylogenetic diversity) and beta-diversity
tances) were performed using PhyloSeq and additional R packages (*39*). Taxa (ASVs) wh
fered significantly between sample groups were identified by performing pairwise comp
MicrobiotaProcess packages (*40*). A correlation matrix was generated and plotted as ell
package (*41*). R codes to generate 16*S* rRNA-related results and figures in this manuscri
https://github.com/shandley/neurodegeneration_16S.

GC-MS of SCFAs

SCFAs were quantified by GC-MS using a previously described protocol (*42*). Cecal cont
placed in 2 mL glass screw cap vials. Ten microliters of a mixture of internal standards
acid-$^{13}C_2$,D_4, propionic acid-D_6, butyric acid-$^{13}C_4$, lactic acid-3,3,3-D_3, and succinic aci
vial, followed by 20 µL of 33% HCl and 1 mL diethyl ether. The solution was vortexed vi
two phases were separated by centrifugation (4000 ×*g* for 5 min). The upper organic lay
other vial and a second 1 ml diethyl ether extraction was performed. After combining th
µL aliquot was mixed with 20 µL N-tert-butyldimethylsilyl-N-methyltrifluoroacetamide
sampler vial with a 200 µL glass insert, and the mixture was incubated for 2 hours at ro
were analyzed in a randomized order. Derivatized samples (1 µL) were injected with 15:
7890A GC system coupled with 5975C MS detector (Agilent). Analyses were carried on a
(30 m × 0.25 mm, 0.25 µm film thickness, Agilent J & W Scientific) using electronic imp
mode. Helium was used as a carrier gas at a constant flow rate of 1.26 mL/min, and the
to 3.5 min. The column head pressure was 10 psi. The temperatures of injector, transfer
270°, 280°, and 150°C, respectively. The GC oven was programmed as follows; 45°C hel
200°C at a rate of 20°C/min, increased to 300°C at a rate of 100°C/min, and finally held

added, and cells were stained for 20 min on ice at 1:300 final dilution. Samples were the buffer and acquired on a spectral flow cytometer (Aurora, Cytek Biosciences). Data were flow software (Cytek) and then gated and quantified using FlowJo v10.8.2 (Treestar).

The following antibodies were used for flow cytometry; anti-CD4 BUV395 (BD, GK1.5, c CD5 BUV496 (BD, 53-7.3, catalog no. 741048), anti-CD27 BUV563 (BD, LG.3A10, catalog BUV615 (BD, IM7, catalog no. 751414), anti-CD11c BUV737 (BioLegend, N418, catalog BUV805 (BD, H57-597, catalog no. 748405), Ly6G BV421 (BioLegend, 1A8, catalog no. 1 Blue (BioLegend, PC61, catalog no. 102022), anti-CD19 BV480 (BD, 1D3, catalog no. 56 (BioLegend, M5/114.15.2, catalog no. 107641), anti-CXCR3 (eBioscience, CXCR3-173, c BV650 (BD, RA3-6B2, catalog no. 563893), anti-CD49a BV711 (BD, Ha31/8, catalog no. (BD, 30-F11, catalog no. 746947), anti-Ly-6C AlexaFluor488 (BioLegend, HK1.4, catalog AlexaFluor532 (eBioscience, 53-6.7m catalog no. 58-0081), anti-CD122 BrilliantBlue70 742112), CD69 PE (BioLegend, H1.2F3, catalog no. 104508), anti-CD186 (CXCR6) PE-Da SA051D1, catalog no. 151117), anti-CD127 PE-Cy5 (BioLegend, A7R34, catalog no. 135 (eBioscience, PK136, catalog no. 108714), anti-TCRg/d AlexaFluor647 (BioLegend,GL3, anti-F4/80 AlexaFluor700 (BioLegend, BM8, catalog no. 123130).

FACS for lung macrophage isolation

Lung samples were harvested from the mice and chopped up with scissors into 1- to 2-r samples were digested in digestion buffer containing 50 U/mL DNase (Sigma), 100 U/m and 0.28 U/mL Liberase (Roche) at 37°C for 45 min. The mixtures were gently inverted a min. A final concentration of 10% FBS was used to stop the reaction and the samples w µm-diameter cell strainer. The cell suspensions were pelleted down by centrifugation a blood cells were removed with 5 mL ACK buffer (150 mM ammonium chloride, 10 mM p 0.1 mM EDTA) at room temperature for 2 min. The reaction was stopped by adding 1 m passed through a 70-µm strainer one more time. Cells were pelleted and ~5 × 10^6 cells v sorting was completed on a FACS AriaII. Staining was performed at 4°C in the presence in magnetic-activated cell-sorting (MACS) buffer (PBS + 0.5% BSA + 2 mM EDTA). The f used from Biolegend: BV510 anti-CD45 (30-F11), APC-Cy7 anti-CD11b (M1/70), Pacific (M5/114.15.2), PercP-Cy5.5 anti-Ly6C/Ly6G (Gr-1) (RB6-8C5), and APC anti-CD64 (X54 from Invitrogen included: PE-Cy7 anti-CD11c (N418) and PE anti-SiglecF (1RNM44N). were sorted as CD45+ SiglecF+ CD11c+ CD64+ $CD11b^{lo}$ cells.

RNA-seq and analysis

RNA was extracted from FACS-sorted lung macrophages (described above) using the RN (QIAGEN, catalog no. 74034). RNA samples were prepared according to library kit manu dexed, pooled, and sequenced on an Illumina NovaSeq 6000. Basecalls and demultiplex Illumina's bcl2fastq2 software. RNA-seq reads were then aligned and quantitated to the mary assembly with an Illumina DRAGEN Bio-IT on-premise server running version 3.9

Cary, NC, RRID:SCR_014242) and GraphPad Prism 9. Means between two groups were c
unpaired Student's *t* test. Comparisons of means from three groups with each other wer
analysis of variance (ANOVA). Two-way ANOVAs were used to analyze between-subject
factors. Repeated-measures designs were analyzed using mixed-effects restricted maxi
model. Tukey was used for post hoc pairwise comparisons. Fisher's exact test was used
tributions. The strength of the linear relationship between two different variables was a
Spearman's correlation. The null hypothesis was rejected at the $P < 0.05$ level. Statistica
$^{*}P < 0.05$, $^{**}P < 0.01$, and $^{***}P < 0.001$. Statistical significance of the main effects witho
variables was indicated as $\#P < 0.05$, $\#\#P < 0.01$, and $\#\#\#P < 0.001$. All statistical inform

Acknowledgments

We thank C. Nagler and her laboratory members at the University of Chicago for the dis
treatment protocol; M. Colonna, Y. Shi, C. Wang, A. Cashikar, J. Long, N. Griffin, M. Cel
and K. de Lima at Washington University for technical discussions; J. Stanley, B. Boros,
Mihindukulasuriya, and L. Wang for technical assistance; D. Bender at CHiiPs (Center f
Immunotherapy Programs at Washington University) for performing multiplex cytokine
Markovic, T. Sinnwell, E. Tycksen, and others at GTAC (Genome Technology Access Cen
University) for their contributions to generating genomic and transcriptomic datasets.

Funding: This study was supported by Good Ventures (D.M.H.) and National Institutes
(D.M.H.).

Author contributions: D.S. played a primary role in conceiving this study, developing
forming experiments, analyzing the resulting datasets, and writing the original draft m
generated and maintained GF mice. N.J. analyzed microglial cell morphology. J.D.U. ana
M.M. extracted DNA from fecal samples and oversaw V4-16*S* rRNA amplicon sequencin
alyzed the resulting 16*S* rRNA datasets. J.H., M.L., and J.K. performed flow cytometry. H
macrophages. J.R.S. and X.B. collected brain, cecum, and plasma samples. E.F. quantifie
S.D. performed metabolomic analyses. J.L.-G., S.S.S., and J.I.G. conceptualized experim
D.M.H. conceptualized, acquired funding for, and supervised the project. J.I.G. and D.M
script.

Competing interests: D.M.H. is a cofounder of C2N Diagnostics, LLC, and is on the sci
and/or consults for Genentech, Denali, C2N Diagnostics, Cajal Neurosciences, and Alec
on a patent licensed by Washington University to C2N Diagnostics on the therapeutic u
and a patent licensed by Washington University to Eli Lilly on a humanized anti-Aβ ant
ratory receives research grants from the National Institutes of Health, Cure Alzheimer'
Foundation, the JPB Foundation, Good Ventures, Novartis, Eli Lilly, and NextCure. The
competing interests.

DOWNLOAD | 5.01 MB

Other Supplementary Material for this manuscript includes the following:

Table S1

DOWNLOAD | 31.18 KB

MDAR Reproducibility Checklist

DOWNLOAD | 155.76 KB

Data S1 to S8

DOWNLOAD | 248.74 KB

View/request a protocol for this paper from *Bio-protocol.*

References and Notes

1 J. M. Long, D. M. Holtzman, Alzheimer Disease: An Update on Pathobiology and Treatment Strategies. *Ce*

GO TO REFERENCE • CROSSREF • PUBMED • ISI • GOOGLE SCHOLAR • Discover full text

2 D. O. Seo, D. M. Holtzman, Gut Microbiota: From the Forgotten Organ to a Potential Key Player in the Pat *Gerontol. A Biol. Sci. Med. Sci.* **75**, 1232–1241 (2020).

GO TO REFERENCE • CROSSREF • PUBMED • ISI • GOOGLE SCHOLAR • Discover full text

3 T. Harach, N. Marungruang, N. Duthilleul, V. Cheatham, K. D. Mc Coy, G. Frisoni, J. J. Neher, F. Fåk, M. Juc

to Alzheimer's, may be at higher risk of ARIA.

Alzheimer's patients aren't routinely tested for ApoE4 because it hasn't traditionally affected Japan, there is concern about the problem of excessive medical treatment, such as the frequer

view more

Deterministic reprogramming of neutrophils within tumors

BY MELISSA S. E. NG, IMMANUEL KWOK, ET AL.

with two copies of the gene variant had sym
ARIA, compared with 1.4% of people with no copies. In short, people with two copies of the A

Pathways toward commercial perovskite/silicon tandem photovoltaics

BY ERKAN AYDIN, THOMAS G. ALLEN, *ET AL.*

Comprehensive conservation assessments reveal high extinction risks across Atlantic Forest trees

BY RENATO A. F. DE LIMA, GILLES DAUBY, *ET AL.*

NEWS | 16 JAN 2024

What does your dog's tail wag really mean?

NEWS | 16 JAN 2024

A promising snakebite treatment seemed ready for prime time. Then, it backfired

SCIENCEINSIDER | 13 JAN 2024

Explosion of violence in Ecuador shuts down science

View full text | Download PDF